Observation of breatherlike states in a single Josephson cell

F. Pignatelli and A. V. Ustinov
Physikalisches Institut III, Universität Erlangen-Nürnberg, Erwin-Rommel-Strasse 1, D-91058 Erlangen, Germany
(Received 27 August 2002; published 14 March 2003)

We present experimental observation of broken-symmetry states in a superconducting loop with three Josephson junctions. These states are generic for discrete breathers in Josephson ladders. The existence region of the breatherlike states is found to be in good accordance with the theoretical expectations. We observed three different resonant states in the current-voltage characteristics of the broken-symmetry state, as predicted by theory. The experimental dependence of the resonances on the external magnetic field is studied in detail.

DOI: 10.1103/PhysRevE.67.036607 PACS number(s): 05.45.Yv, 85.25.Cp, 63.20.Pw, 05.45.Xt

I. INTRODUCTION

Nonlinearity and discreteness in lattices lead to the existence of spatially localized stable solutions [1–3]. These solutions, called discrete breathers (DBs), are characterized by time periodicity and a strong spatial localization of energy, of the scale of the lattice constant. The localized mode can be vibrational or rotational, depending on the lattice and the type of excitation. In the second case, the DB is called *rotobreather*. DBs were found to exist in a large variety of nonlinear discrete lattices, including weakly coupled optical wave guides [4], crystal lattice in solids [5], antiferromagnets [6], and Josephson junction arrays [7–11]. The latter system is a convenient experimental tool to investigate the existence and dynamics of DBs. The discrete lattice used here is constituted by an array of coupled underdamped small Josephson junctions (JJs).

A JJ is composed of two superconducting layers separated by a thin tunnel barrier. Its dynamics can be described in the resistively-capacitively-shunted-junction model (RCSJ) [12]. The equation for the superconducting phase difference between the two superconducting layers constituting the junction φ is written in the normalized form as

$$\gamma = \ddot{\varphi} + \alpha\dot{\varphi} + \sin\varphi. \tag{1}$$

Here the time unit is normalized by the inverse of the Josephson plasma frequency ω_p, γ is the bias current I normalized by its critical value and α is the damping. This equation is formally equivalent to the equation of motion of a weakly damped pendulum in the presence of an external torque γ. This mechanical analog allows an easy description of the two possible states of the JJ. If we apply a torque $\gamma > 1$, the pendulum will start to rotate with an average frequency $\langle\dot{\varphi}\rangle$. After the pendulum is driven to the rotating state, it will stay in this state, even for $\gamma < 1$, as long as the external torque is large enough to compensate the damping term. So that, at some range of γ, both static and rotating states are possible, depending on the initial conditions. By the second Josephson equation $V = \Phi_0/2\pi\langle\dot{\varphi}\rangle$, these two states are equivalent, respectively, to the superconducting and resistive states of the JJ. In experiment, by measuring the voltage on the JJ, it is possible to distinguish between these two states.

Josephson ladders allow for the existence of both oscillatory and rotational localized modes [13]. However, only the latter ones are easy to detect experimentally. A rotobreather in the Josephson ladder is constituted by some of the JJs in the resistive (rotating) state, while the rest of JJs stay in the superconducting (oscillating) state. The rotobreathers were experimentally detected by measuring the *I-V* characteristics of the JJs in different points of the ladder [7,10] and were also directly visualized by low temperature scanning laser microscopy [8,9].

Josephson ladders can support linear cavity modes that can interact with the localized modes [10,11,14,15]. The interaction of the linear modes of the ladder with the localized modes was found to lead to nonlinear features in the characteristic of DBs. Their complex dynamics in the region of the linear cavity resonances was investigated experimentally by the measurements of the *I-V* characteristics of various DBs [11].

Single Josephson cells have been proposed [16,17] to provide an insight into complex discrete breather states of larger systems such as Josephson ladders and two-dimensional Josephson junction arrays. Broken-symmetry states with characteristics similar to those of discrete breathers were proposed to exist [16–18]. In the following, we will call these broken-symmetry states *breatherlike* states.

Superconducting loops with three Josephson junctions have also been recently proposed for the realization of a qubit [19,20]. Such a loop has an important property required for the qubit, namely, two closely positioned minima in the dependence of its energy on the external magnetic field [21]. Note, however, that in this work we are interested in phase-rotational states, which are clearly different from oscillatory states discussed for qubits.

In this paper, we study a single Josephson cell with three small underdamped Josephson junctions. Two junctions of same area placed along the direction parallel to the uniform bias current, V_1 V_2, are called vertical junctions. The third junction located in one of the two transverse branches of the cell, is called horizontal *H*, see Fig. 1.

A parameter of cell *anisotropy*, η, is defined as the ratio between the critical current of the horizontal junction and one of the vertical junctions, $\eta = I_{CH}/I_{CV}$. The parameter of anisotropy describes the coupling between the two vertical junctions, so that, in the limit $\eta \to 0$, the two vertical junctions are entirely decoupled, while the larger the η is, the

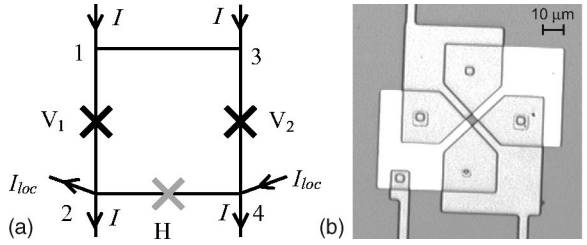

FIG. 1. (a) Sketch of the single Josephson cell, with three JJs (indicated by crosses), two vertical V_1, V_2 and one horizontal H. (b) Optical image of our experimental cell with 4×4 μm^2 hole and three underdamped Nb/Al-AlO$_x$/Nb JJs.

stronger is the coupling. The cell is called isotropic if all three junctions have same parameters, anisotropic otherwise. The system is uniformly biased by two equal currents I, applied through the vertical branches, 1-2 and 3-4, Fig. 1. As long as the uniform bias current I is smaller than the critical current I_{CV}, all the junctions stay in the superconducting state, Fig. 2(a). As the current I exceeds the critical value I_{CV}, the system switches to the homogeneous whirling state, constituted by both vertical junctions in the resistive state and the horizontal one in the superconducting state, Fig. 2(b). Both these cases are symmetric states and there is no current on the horizontal junction, so that the two vertical junctions behave identically. We are interested in the last two cases, Figs. 2(c) and 2(d), which are the inhomogeneous breatherlike states. These two states have the same behavior and are characterized by the horizontal junction and one of the vertical junctions in the resistive state, while the other vertical junction remains in the superconducting state. In these cases, obviously, some part of the bias current flows through the transverse branch.

The procedure to generate breatherlike states in experiments is similar to that used for Josephson ladders [7,8]. We bias the system by a local current I_{loc} through the transverse branch 4-2, Fig. 1, and increase this current until the system switches to a breatherlike state. Afterwards, we increase the bias current I and simultaneously decrease I_{loc} to zero, keeping the system in the generated state. An alternative procedure is to first apply a homogeneous bias current $I<I_{CV}$ at a value where we expect to find the breatherlike state stable, then increase the local current I_{loc} to generate it, and finally reduce I_{loc} back to zero. By using the two different directions of the initial local current, it is possible to generate both breatherlike states shown in Fig. 2.

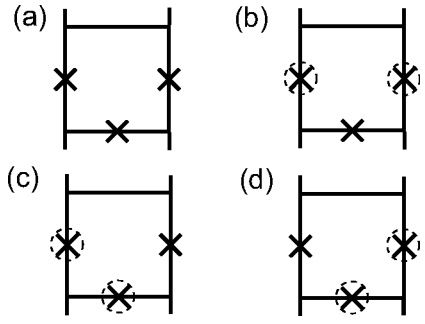

FIG. 2. Possible states of the system: (a) superconducting state, (b) homogeneous whirling state, and (c) and (d) the two symmetric breatherlike states.

Different states of the system can be experimentally detected by measuring the dc voltage on Josephson junctions. As for Josephson ladders, the broken-symmetry states are the consequence of the characteristic property of small underdamped Josephson junctions, that is, the coexistence, for some ranges of the bias current, of two different stable states, superconducting and resistive.

II. DYNAMICS OF THE SYSTEM

The dynamics of the system is described by the phase differences across the three Josephson junctions φ_{V_1}, φ_{V_2}, φ_H. Using the current conservation law in each node of the cell and the flux quantization for the cell, one can get the equations of motion for the system [17,18]:

$$\mathcal{N}(\varphi_{V_1})=\gamma-\frac{1}{\beta_L}(\varphi_{V_1}-\varphi_{V_2}+\varphi_H+2\pi f),$$

$$\mathcal{N}(\varphi_{V_2})=\gamma+\frac{1}{\beta_L}(\varphi_{V_1}-\varphi_{V_2}+\varphi_H+2\pi f),$$

$$\mathcal{N}(\varphi_H)=-\frac{1}{\beta_L\eta}(\varphi_{V_1}-\varphi_{V_2}+\varphi_H+2\pi f), \qquad (2)$$

where the time is normalized by the inverse of the Josephson plasma frequency ω_p. The influence of the external magnetic field is introduced by the term $2\pi f/\beta_L$. The parameters of the system are the uniform *bias current* normalized by the critical current of the vertical junctions, $\gamma=I/I_{CV}$, the normalized *self-inductance* of the cell, $\beta_L=2\pi LI_{CV}/\Phi_0$ (where L is its real inductance), the *damping*, $\alpha=\sqrt{\Phi_0/(2\pi I_C R^2 C)}$, and the frustration parameter $f=\Phi_{ext}/\Phi_0$, which can be tuned by the external magnetic field H. The operator $\mathcal{N}$ represents the current through a single junction in the RCSJ model and is defined as $\mathcal{N}(\varphi)=\ddot{\varphi}+\alpha\dot{\varphi}+\sin\varphi$.

Using a simplified dc model [17], where the vertical and horizontal junctions in the resistive state are considered as resistances (R_V for vertical junctions and $R_H=R_V/\eta$ for horizontal ones) and those in the superconducting state just as shorts, one can estimate the dimensionless breather frequency $\Omega=\langle\dot{\varphi}\rangle$, that is the voltage across a junction in the resistive state normalized by $\Phi_0\omega_p/2\pi$:

$$\Omega=\frac{\gamma}{\alpha(1+\eta)}. \qquad (3)$$

From this one can also evaluate the region of existence of the breatherlike state. The minimum current γ_r at which a broken-symmetry state may exist is $\gamma_r=(1+\eta)\gamma_R$, where γ_R is the retrapping current of the single junction. According to Ref. [22], $\gamma_R=4\alpha/\pi$ and

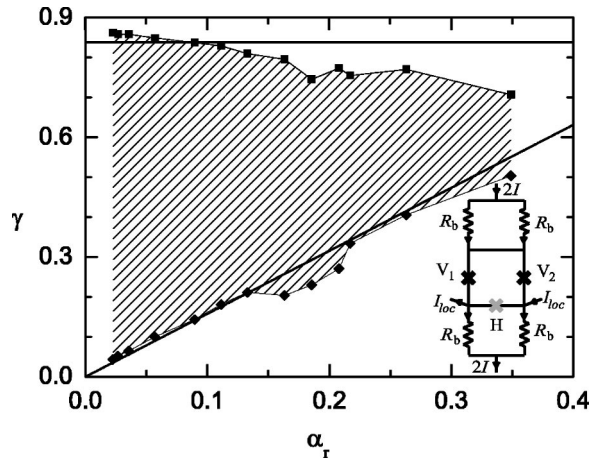

FIG. 3. Dependence of maximum (solid squares) and minimum (solid diamonds) currents for the breatherlike state on the damping α_r. The solid lines show the theoretical expectations of the dc model, Eqs. (4) and (5). The inset shows the sketch of the system with the biasing circuit.

$$\gamma_r = \frac{4\alpha}{\pi}(1+\eta). \tag{4}$$

At $\gamma < \gamma_r$ the system is retrapped to the superconducting state. The maximum current for a breatherlike state is

$$\gamma_c = \frac{1+\eta}{1+2\eta}. \tag{5}$$

Above this current the system switches to the homogeneous rotating state.

In experiment the bias current $2I$ is introduced in parallel via two external resistors R_b, see inset in Fig. 3. In a broken-symmetry state this biasing scheme induces a nonequal bias currents in the two vertical branches. This leads to a reduction of the breather frequency,

$$\tilde{\Omega} = \frac{\gamma}{\alpha[(1+\eta)+r]} \simeq \Omega\left(1 - \frac{1}{1+\eta}r\right). \tag{6}$$

With $r = R_V/2R_b$ the region of existence of the breather states shrinks to $\widetilde{\gamma_r} < \gamma < \widetilde{\gamma_c}$, where

$$\widetilde{\gamma_r} = \gamma_r + \frac{4\alpha}{\pi}r,$$

$$\widetilde{\gamma_c} = \frac{(1+\eta)+r}{(1+2\eta)+2r} \simeq \gamma_c - \frac{1}{(1+2\eta)^2}r. \tag{7}$$

The I-V characteristic of a small underdamped JJ is strongly nonlinear. Therefore the damping α strongly depends on Ω. The value of r and the discussed corrections, Eqs. (6) and (7), are large only in the subgap voltage range, where R_V is large. For simplicity we will assume $\widetilde{\gamma_c} = \gamma_c$. The bias resistors also influence the damping in the horizontal JJ. Roughly speaking, we have to consider an additional resistance $2R_b$ in parallel to the horizontal JJ. This leads to a correction of damping in the horizontal JJ to $\tilde{\alpha} = \alpha(1 + r/\eta)$. Note that this simplified analysis is valid only for dc currents. At high frequencies the shunting effect of R_b is reduced due to the large inductance of the bias leads.

The simplified dc model neglects the influence of the small oscillations of the Josephson phase that may cause instability and nonlinearity in the characteristics of the breatherlike state. Neglecting the damping and linearizing the equation of motion, Eqs. (2), around the breatherlike state, Eq. (3), it is possible to calculate the two characteristic frequencies of these oscillations [17,18]:

$$\omega_\pm = (F \pm \sqrt{F^2 - G})^{1/2}, \tag{8}$$

where

$$F = \frac{1}{2}\cos(c_1) + \frac{1+2\eta}{2\eta\beta_L},$$

$$G = \frac{1+\eta}{\eta\beta_L}\cos(c_1).$$

Here c_1 is the phase shift of the vertical junction in the superconducting state evaluated by the dc model, $c_1 = \arcsin[\gamma(1+2\eta)/(1+\eta)]$. The presence of the electromagnetic oscillations leads then to *primary* resonances in the breatherlike state, when the frequency of the breather Ω locks to the frequency of the electromagnetic oscillations ω_+ or ω_-, and to *parametric* and *combination* resonances, respectively, at $\Omega = n\omega_\pm$, where $n \geqslant 2$ is an integer, and $\Omega = n(\omega_+ \pm \omega_-)$, where n is an integer [17,18].

Using the rotational approximation [23], two different dependences of the resonant step amplitude $\Delta\gamma$ on the frustration have been obtained for *primary* and *parametric* resonances [18]:

$$\Delta\gamma_{\omega_\pm} \propto \left|\sin\left(\frac{c_1}{2} + \frac{\beta_L\gamma\eta}{2(1+\eta)} + \pi f\right)\right|, \tag{9}$$

$$\Delta\gamma_{n\omega_\pm} \propto \sqrt{(1-\eta)^2 + 4\eta\cos^2\left(\frac{c_1}{2} + \frac{\beta_L\gamma\eta}{2(1+\eta)} + \pi f\right)}. \tag{10}$$

Expressions (9) and (10) have the same periodicity in f as the critical current in the whirling state, but, depending on the parameters of the system, they may be asymmetric with respect to $f = 0$. Moreover, the external magnetic field can considerably change the amplitude of the resonance and, in the case of primary resonance, even make it vanish for some values of the frustration.

III. EXPERIMENTAL RESULTS

Our experimental system is a single cell with the hole area $4 \times 4\ \mu\text{m}^2$, containing three small underdamped Nb/Al-AlO_x/Nb Josephson junctions [24], see Fig. 1. The critical current density, measured at 4.2 K, is $J_C = 133\ \text{A/cm}^2$. The area of each vertical junction is about $7 \times 7\ \mu\text{m}^2$, while that of horizontal one is $3 \times 4\ \mu\text{m}^2$. The

anisotropy of the system, evaluated from the design, is then $\eta = 0.24$. The parameter of self-inductance of the cell at 4.2 K, evaluated by measurement of a superconducting quantum interferences device (SQUID) of same geometry, is $\beta_L = 1.47$. The two equal bias currents are introduced by two parallel external resistances, $R_b = 1.5\ \mathrm{k}\Omega$. This leads to r parameter ranging between 0.35 and 0.02, depending on T, so that the corrections of Eqs. (6) and (7) are negligible. The measurements are performed in a ^{4}He cryostat [25] in the temperature range between 4 K and 8 K, so that the parameters of the system J_C, α, β_L, and ω_p can be varied. For each temperature the subgap damping $\alpha_{sg} = \sqrt{\Phi_0/(2\pi I_{CV} R_{sg}^2 C)}$ is evaluated from the subgap resistance R_{sg} of the homogeneous whirling state (for $\Omega < 16$). The effective damping in the RCSJ model, $\alpha_r = (\pi/4) \times (I_R/2I_{CV})$, and the critical current density J_C are evaluated from the characteristic of the homogeneous whirling state at various temperatures, while the parameter of self-inductance β_L is evaluated from the critical current density. Finally, the value of the plasma frequency is obtained at every temperature by fitting the voltage of the parametric resonant step to the expected value $2\omega_+$.

For the convenience of comparing with theory, the experimental data are shown in the previously introduced normalized units of the bias current $\gamma = I/I_{CV}$, breather frequency $\Omega = V/(\omega_p \Phi_0/2\pi)$, and frustration $f = \Phi_{ext}/\Phi_0$.

In the range of temperatures from 4.2 K to 7.75 K it was possible to excite both breatherlike states and they were found stable in a finite range of the bias current. No breatherlike state was found stable for temperatures above 7.75 K ($\alpha_r > 0.35$).

In Fig. 3 the experimental dependence of the current region of existence of the broken-symmetry states on the effective damping α_r is reported. The bias current at which the breather is retrapped, γ_r, increases linearly with the damping, in good agreement with the theoretical expectation of Eq. (4). The maximum current that allows the existence of the breatherlike state slightly decreases with increasing damping α_r, see Fig. 3, whereas from Eq. (5) it is expected to be constant ($\gamma_c = 0.84$).

In fact, the temperature variation leads to an alteration of several parameters, see Fig. 4. In particular, the decrease of the self-inductance β_L at high temperatures leads to stronger interactions of the breatherlike state with the small oscillations. This effect may strongly affect (in the range $0.1 < \beta_L < 1$) the region of existence of the breatherlike state, especially its upper border [17]. In fact, the experimental data show deviation from the expected value for $\alpha_r \geqslant 0.15$, which is in the range of the self-inductance between 0.9 and 0.3.

The values of damping, α_r and α_{sg}, and of the respective resistances, R_r and R_{sg}, are shown in Fig. 4. The difference between the two resistances is about a factor 10 and follows from the models that describe the whirling state in the subgap branch [26–28]. R_{sg} allows for a phenomenological description of the dynamics, assuming the damping is constant, dotted line in Fig. 5. R_r gives an estimation of the equivalent resistance responsible for the effective dissipation in the generalized RCSJ model proposed by Chen, Fisher, and Leggett [26]. Following this model, the I-V characteristic near the

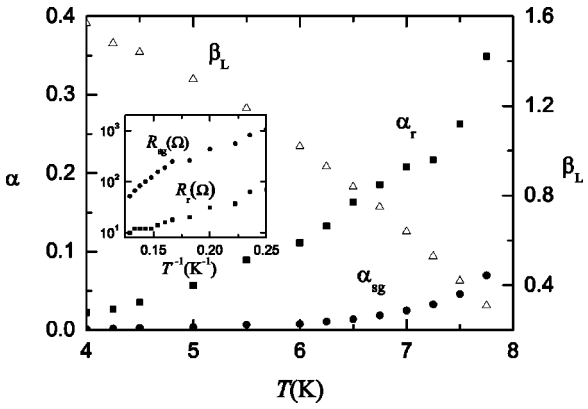

FIG. 4. Dependence of the damping, evaluated by the retrapping current (α_r solid squares) and by the subgap resistance (α_{sg} solid circles), and of the self-inductance (open triangles) on the temperature of the system. The inset shows the subgap resistance R_{sg} and the effective resistance R_r, vs T^{-1}.

retrapping current ($\gamma - \gamma_r \ll \gamma_r$) is described by the formula $\gamma - \gamma_r = \gamma_r[(2\pi A/\Omega) + B]\exp(-2\pi/\Omega)$, where A and B are constants, see the fit shown by a solid line in Fig. 5. The temperature dependence of the two resistances is similar and agrees with the theoretical expected behavior for the thermal regime, $R \propto \exp(\Delta/k_B T)$, where Δ is the energy gap and k_B is the Boltzman constant [26], see inset in Fig. 4.

No resonances were observed in the I-V characteristics at temperatures below 6 K. The small damping of the junctions at this temperature seems to be unfavorable for reaching the small frequencies of the electromagnetic oscillations where the resonances are expected ($\Omega_{min} \simeq 5.5$). Increasing the temperature of the system had two helpful effects for seeing the resonances, namely, the increase in damping and decrease in self-inductance, see Fig. 4. As a consequence of the larger damping, the breatherlike states were stable down to smaller frequencies, whereas a smaller inductance moved the frequencies of the resonances up.

At $T = 6$ K it was possible to observe the first resonant step. The parameters of the system at this temperature are

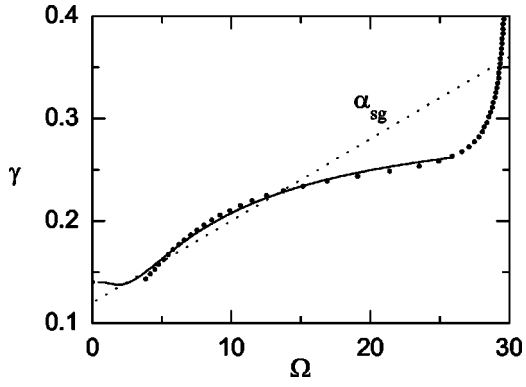

FIG. 5. Measured subgap branch for the whirling state (solid circles) at $T = 6$ K and its fit (solid line) by the formula $\gamma - \gamma_r = \gamma_r[(2\pi A/\Omega) + B]\exp(-2\pi/\Omega)$ with $A = -0.53$ and $B = 1.24$ [26]. The dotted line shows the phenomenological model $\gamma = \gamma_0 + \alpha_{sg}\Omega$.

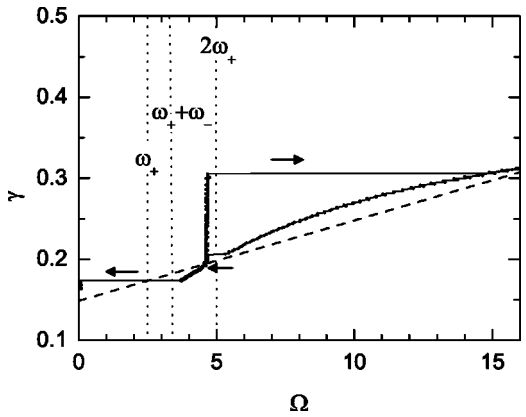

FIG. 6. Measured current-voltage characteristics of the breatherlike state at temperature $T=6$ K and frustration $f=-0.1$, where the magnitude of the resonant step is maximum. The dashed and dotted lines show, respectively, the theoretical expectations for the current-voltage curve, Eq. (3), and for the frequencies of the resonances, Eq. (8).

$\alpha_r \simeq 0.11$, $\alpha_{sg} \simeq 0.008$, $J_c = 92$ A/cm^2, $\beta_L = 1.02$, and $\omega_p/2\pi = 37$ GHz. This resonance is a step in the characteristic, shown in Fig. 6. Comparing this resonance with that at higher temperatures and with the theoretical expectation, we deduce it to be the parametric resonance at $2\omega_+$.

At $T=6.65$ K we detect two additional resonances in the characteristics of the breatherlike state, see Fig. 7. At this temperature the parameters of the system are $\alpha_r \simeq 0.18$, $\alpha_{sg} \simeq 0.016$, $J_c = 70$ A/cm^2, $\beta_L = 0.77$ and $\omega_p/2\pi = 30$ GHz. The two larger resonances, *A* and *B*, are different by an integer factor of 2, as expected for $2\omega_+$ and ω_+. The dependences of the current amplitude on the external magnetic field for steps *A* and *B* is strongly different. The resonance *A* has its maximum amplitude close to zero frustration, see Fig. 7(a), and disappears in a wide range around $f=0.5$, see Fig. 8. Another resonance *B* is always present, but has nearly opposite behavior. At the top of the resonance *B*, around frustration $f=0.4$ or $f=-0.6$, the system shows an instability by switching either to the homogeneous whirling state or to the superconducting state, as shownin Fig. 8. In this range of frustration the measurements of the resonant step *B* were performed with less accuracy and faster because of its poor stability. We argue that the larger step *B* is due to the primary resonance at $\Omega=\omega_+$, whereas the step *A* is due to the parametric resonance at $\Omega=2\omega_+$. The third smaller nonlinearity *C* is at a frequency between the other two, close to the theoretically expected value for the combination resonance at $\Omega=\omega_+ + \omega_-$, see Fig 7. This resonance was only present in a small range of frustration around zero, where, from the theory, the combination resonance is expected to be maximum. Because of its reduced amplitude this resonant step has no hysteresis and its dependence on the magnetic field was not measured.

In Figs. 9(b),9(c) we present measurements of the current amplitude of the resonant steps *A* and *B* on the external magnetic field. The parametric step at $T=6$ K, see Fig. 6, is higher than that at $T=6.65$ K, Fig. 7. Moreover, because of the larger damping in the latter case the step vanishes in a larger range of the frustration ($-0.95<f<-0.25$ and $0.05<f<0.75$). Therefore, in order to observe a more clear modulation of this resonance, we report in Fig. 9(c) its dependence on the external magnetic field at $T=6$ K.

As expected from theory, Eqs. (9) and (10), the magnetic field dependence of the resonance amplitudes show an asymmetry with respect to $f=0$. Note that such asymmetry is not observed for $I_C(f)$, see Fig. 9(a). The asymmetry depends on the parameter of the system and particularly on the bias current where the resonance occurs. This behavior can be qualitatively attributed to the current flowing in the transverse branch of the cell in the broken-symmetry state. The experimental data are in rather good agreement with the theoretical expectations. We fitted the maximum and minimum of the resonant steps in order to find the proportionality coefficient in Eqs. (9) and (10). The small variations of the experimental data around the maximum of the primary resonant step could be due to the appearance of instabilities, as discussed in relation to Fig. 8. This behavior was also found in simulations [18]. In the case of parametric resonance, the presence of a range of frustration, which increases with the damping α, where resonant step disappears, is also expected [18]. Note that the region where the experimental data show the largest

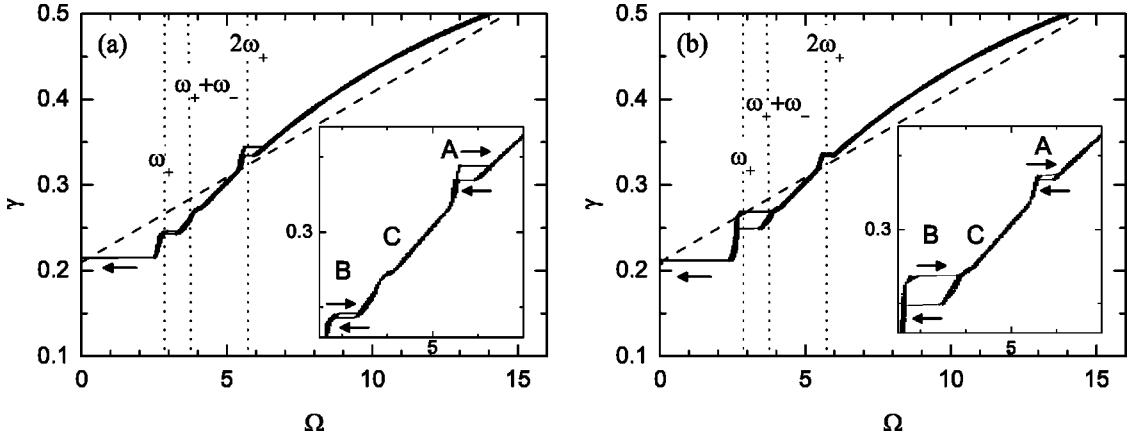

FIG. 7. Measured current-voltage characteristics of the breatherlike state at temperature $T=6.65$ K and for (a) $f=-0.1$, (b) $f=0$. The dashed and dotted lines are explained in Fig. 6. The insets show a magnified view the region of interest.

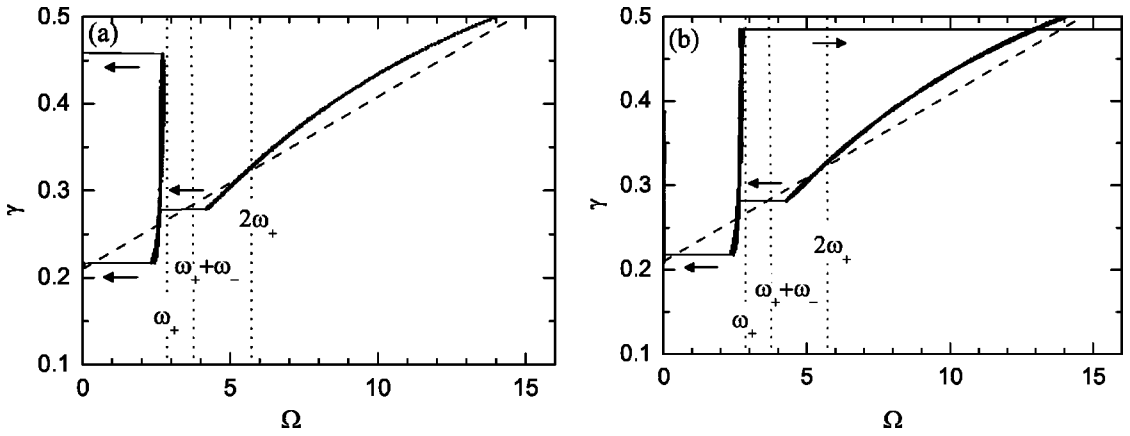

FIG. 8. Measured current-voltage characteristic of the breatherlike state in presence of instabilities at temperature $T=6.65$ K (a) $f=-0.6$, (b) $f=0.4$. The dashed and dotted lines are explained in Fig. 6.

deviation from the expected behavior is nearly the same for the two cases ($-0.7<f<-0.4$,$0.3<f<0.6$).

IV. CONCLUSIONS

We observed breatherlike states of broken symmetry in an anisotropic single-cell system. For temperatures lower than 6 K, the current-voltage characteristics of the breatherlike states were stable and did not show any resonances. Increasing the dissipation by raising the temperature of the system, we decreased the frequencies of rotation of the breatherlike state in such a way that it matched the frequencies of the resonances in the cell. In this region, the primary, combination, and parametric resonances were observed. As expected, for all three cases, the interaction of the electromagnetic oscillations with the breatherlike state leads to resonant steps in the current-voltage characteristic. The large steps due to the primary and parametric resonances show hysteresis, whereas the combination one induces just a small nonlinearity in the characteristic. The measured dependence on the external

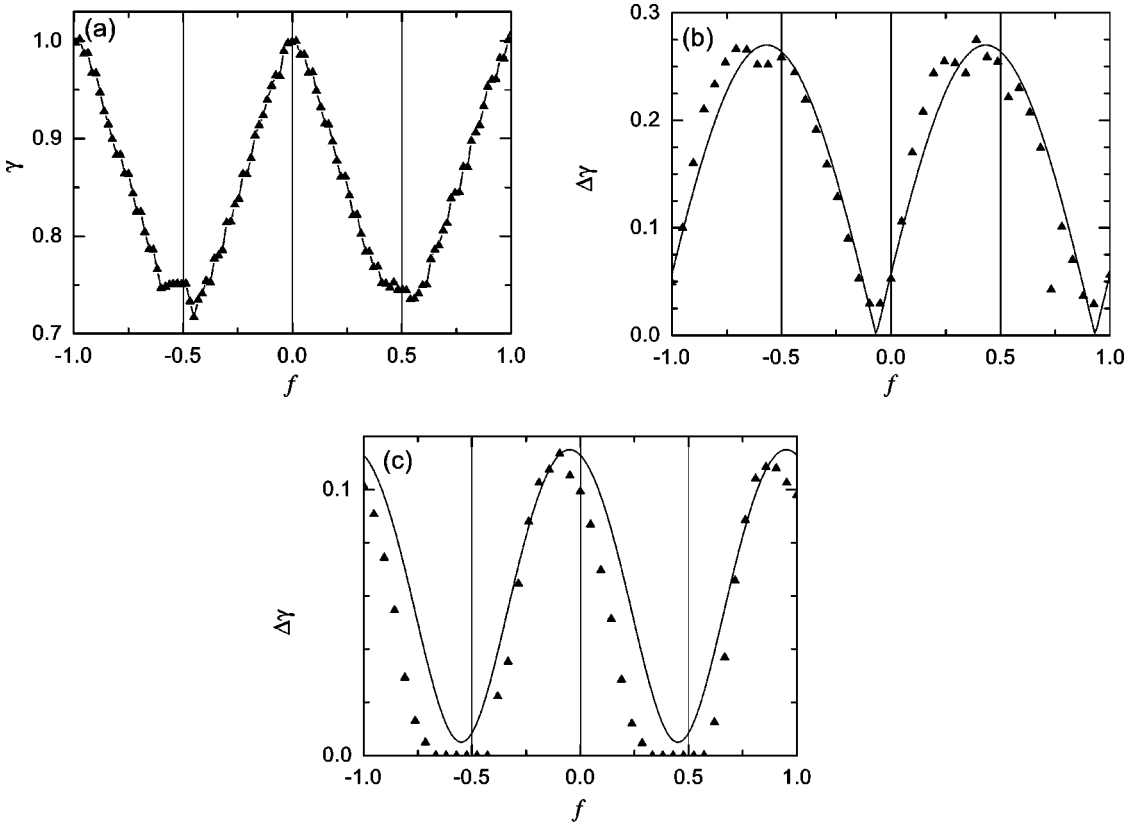

FIG. 9. (a) Dependence of the critical current of the homogeneous state on the frustration. (b) and (c) show dependence of the magnitude of the resonant step on the frustration for primary resonance A (measured at $T=6.65$ K) and parametric resonance B (measured at $T=6$ K), respectively. The solid lines are the theoretical curves given by Eqs. (9) and (10), respectively.

magnetic field of the magnitude of the primary and parametric resonant steps is in good agreement with theory. In the case of primary resonance, the external frustration strongly increases the amplitude of the resonant step and leads to instability of the breatherlike state. The combination resonance, for the same values of the damping, was present just in a small range around zero frustration and did not lead to instabilities. The region of existence of the breatherlike state was also measured and found in good accordance with the expectations. At smaller values of the self-inductance parameter the stronger interaction of the breather with the electromagnetic oscillations leads to a contraction of the region of existence.

ACKNOWLEDGMENTS

We would like to thank A. Benabdallah, P. Binder, M. V. Fistul, S. Flach, A. E. Mirishnichenko, and M. Schuster for the fruitful discussions and for sending us their latest works before publication. This work was supported by the Deutsche Forschungsgemeinschaft (DFG) and by the European Union under RTN project LOCNET HPRN-CT-1999-00163.

[1] S. Takeno and M. Peyrard, Physica D **92**, 140 (1996).
[2] S. Aubry, Physica D **103**, 201 (1997).
[3] S. Flach and C.R. Willis, Phys. Rep. **295**, 181 (1998).
[4] H.S. Eisenberg, Y. Silberberg, R. Morandotti, A.R. Boyd, and J.S. Aitchison, Phys. Rev. Lett. **81**, 3383 (1998).
[5] B.I. Swanson, J.A. Brozik, S.P. Love, G.F. Strouse, A.P. Shreve, A.R. Bishop, W.-Z. Wang, and M.I. Salkola, Phys. Rev. Lett. **82**, 3288 (1999).
[6] U.T. Schwarz, L.Q. English, and A.J. Sievers, Phys. Rev. Lett. **83**, 223 (1999).
[7] E. Trías, J.J. Mazo, and T.P. Orlando, Phys. Rev. Lett. **84**, 741 (2000).
[8] P. Binder, D. Abraimov, A.V. Ustinov, S. Flach, and Y. Zolotaryuk, Phys. Rev. Lett. **84**, 745 (2000).
[9] P. Binder, D. Abraimov, and A.V. Ustinov, Phys. Rev. E **62**, 2858 (2000).
[10] E. Trías, J.J. Mazo, A. Brinkman, and T.P. Orlando, Physica D **156**, 98 (2001).
[11] M. Schuster, P. Binder, and A.V. Ustinov, Phys. Rev. E **65**, 016606 (2002).
[12] A. Barone and G. Paternó, *Physics and Applications of the Josephson Effect* (Wiley, New York, 1982).
[13] L.M. Floria, J.L. Marín, P.J. Martínez, F. Falo, and S. Aubry, Europhys. Lett. **36**, 539 (1996).
[14] A.E. Miroshnichenko, S. Flach, M.V. Fistul, Y. Zolotaryuk, and J.B. Page, Phys. Rev. E **64**, 066601 (2001).
[15] M.V. Fistul, A.E. Miroshnichenko, S. Flach, M. Schuster, and A.V. Ustinov, Phys. Rev. B **65**, 174524 (2002).
[16] J.J. Mazo, E. Trías, and T.P. Orlando, Phys. Rev. B **59**, 13 604 (1999).
[17] A. Benabdallah, M.V. Fistul, and S. Flach, Physica D **159**, 202 (2001).
[18] M.V. Fistul, S. Flach, and A. Benabdallah, Phys. Rev. E **65**, 046616 (2002).
[19] T.P. Orlando, J.E. Mooij, L. Tian, C.H. van der Wal, L.S. Levitov, S. Lloyd, and J.J. Mazo, Phys. Rev. B **60**, 15 398 (1999).
[20] S.P. Yukon, Physica C **368**, 320 (2002).
[21] S. P. Yukon (private comunication).
[22] K. K. Likharev, *Dynamics of Josephson Junctions and Circuits* (Gordon and Breach, Pennsylvania, 1986).
[23] I.O. Kulik, Sov. Phys. Tech. Phys. **12**, 111 (1967).
[24] HYPRES Inc., Elmsford, NY 10523.
[25] E.T. Swartz, Rev. Sci. Instrum. **57**, 2848 (1986).
[26] Y.C. Chen, M.P.A. Fisher, and A.J. Leggett, J. Appl. Phys. **64**, 3119 (1988).
[27] P. Silvestrini, O. Liengme, and K.E. Gray, Phys. Rev. B **37**, 1525 (1988); P. Silvestrini, *ibid.* **46**, 5470 (1992).
[28] R. Cristiano, L. Frunzio, C. Nappi, M.G. Castellano, G. Torrioli, and C. Cosimelli, J. Appl. Phys. **81**, 7418 (1997); M.G. Castellano, G. Torrioli, F. Chiarello, C. Cosimelli, and P. Carelli, *ibid.* **86**, 6405 (1999).